

# Self-powered wind sensor based on triboelectric nanogenerator for detecting breeze vibration on electric transmission lines

Xiaolong Tang, Wenchu Hou, Qiwei Zheng, Lin Fang, Rui Zhu\*, Li Zheng\*

*College of Mathematics and Physics, Shanghai Key Laboratory of Materials Protection and Advanced Materials in Electric Power, Shanghai University of Electric Power, Shanghai 200090, China*

## ARTICLE INFO

### Keywords:

Breeze vibration  
Triboelectric nanogenerator  
Non-contact electrification  
Wind speed and direction sensor  
Transmission lines

## ABSTRACT

Overhead transmission lines are susceptible to ambient wind and are easily damaged by long-term breeze vibration. Self-powered systems based on triboelectric nanogenerator (TENG) provide a way to monitor ambient wind conditions over long distances at any time. In this work, a wind monitoring TENG (WM-TENG) is proposed to match the natural environmental conditions that tend to cause breeze vibrations. Non-contact electrostatic induction is applied to avoid abrasion caused by rigid surface contact. The ambient wind speed and wind direction posed on transmission lines are monitored by the top and bottom part of WM-TENG, respectively. Cooperated with our home-designed program, the WM-TENG is used to record and analyze the accumulated duration caused by breeze vibration on transmission lines. This design expands the applications of TENG on transmission lines, and is expected to be applied in long-distance power grids.

## 1. Introduction

As the main carrier in the transmission and distribution of electrical energy, the overhead transmission lines play an important role in social life and economic development [1]. Transmission lines are designed at a high height away from the ground for the safety of the surrounding environment and equipment [2,3], thus can be easily damaged by the wind-induced phenomenon of Carmen vortex that will cause breeze vibration [4–6]. The wind with a speed of 0–5 m/s and a direction of 45°~90° is most likely to cause this phenomenon [7]. Long-term breeze vibration is a huge potential and irreversible danger to transmission lines, and generally its invisibility has already made grid security compromised when it is discovered [8]. The usual preventive approach is to record the durations of breeze vibrations and replace the transmission line before the line is damaged by breeze wind. Therefore, in order to ensure the safety of transmission lines, trillions of distributed sensors need to be deployed to monitor the operation of the grid [9]. However, it is difficult for sensors to obtain electricity directly from electric transmission lines. If batteries are used, the problems of frequent replacement and environmental pollution will become prominent [10, 11]. Thanks to the invention of triboelectric nanogenerator (TENG), which can harvest various mechanical energies in the surrounding environment into electrical energy [12–19], the power supply problem

can be solved. In addition, TENG have advantages of low cost, flexible structures, wide material choices [20–22], various application fields [23–26], which is expected to solve the difficulties encountered in transmission line monitoring.

Most previous wind-related TENG converts wind energy into electricity and transmits data wirelessly when enough energy is collected [27–29]. In the process of collecting wind energy, the output power of TENG is found to be related to wind speed [30–32]. Therefore, wind speed monitoring using TENG has received extensive attention. Due to the complex changes in wind direction, monitoring it through delicately structured TENGs still remains a challenge [33–35]. Moreover, the adaptability to environment and abrasive resistance also put limitation on the TENG-based devices [36–38].

In this work, a self-powered wind monitoring TENG (WM-TENG) is proposed that can monitor both the direction and speed of wind for the main conditions that cause breeze vibrations on electric transmission lines in real time. It uses a non-contact design to avoid the abrasion of contact-induced material during movements, and uses a sponge to replenish charges to compensate for the dissipation of charges. With these two approaches, the surface charge density can be ensured while extending the device lifetime [39–41]. In addition, the monitoring of wind speed and constant wind direction is demonstrated on a home-designed programmable software, which has perfect real-time

\* Corresponding authors.

E-mail addresses: [zhurui@shiep.edu.cn](mailto:zhurui@shiep.edu.cn) (R. Zhu), [zhengli@shiep.edu.cn](mailto:zhengli@shiep.edu.cn) (L. Zheng).



monitoring capabilities and can statistically measure the duration of breeze vibrations. This system does not require complex control circuits and can reduce power burden of the monitored transmission lines. Our work provides a new way for the practical application of TENG in the field of remote transmission lines.

## 2. Experimental sections

### 2.1. Fabrication of the wind sensor system

During the preparation of the TENG, a laser cutter was used to cut a 3 mm thick acrylic plate into a disk as a substrate. White PLA materials are used to print the other parts through a 3D printer (FLASHFORGE Adventurer3), such as dielectric layer supporters, connection sleeves, blades and vanes, etc. The dielectric layer is supported in a fan shape of 15.5–65 mm and an angle of 19.5°, and the aluminum electrode is pasted on its surface and fixed radially on the substrate. Different numbers of sponges are pasted on the substrate according to the requirements, and the integration is called as the fixed part. Teflon film is attached to another support in the same size, which is integrated with the sleeve, vanes or blades, called as the moving part, as shown in Fig. S1. To reduce rigid abrasion, the PTFE and Al are vertically separated by 1.5 mm through printed spacers. The moving part and the fixed part are set on the central shaft, as shown in Fig. S2.

### 2.2. Electrical output measurements

For performance evaluation, the open-circuit voltage and short-circuit current of TENG devices were measured by a programmable LabVIEW platform. It consists of a Keithley 6514 electrometer and an NI USB 6363 data acquisition device.

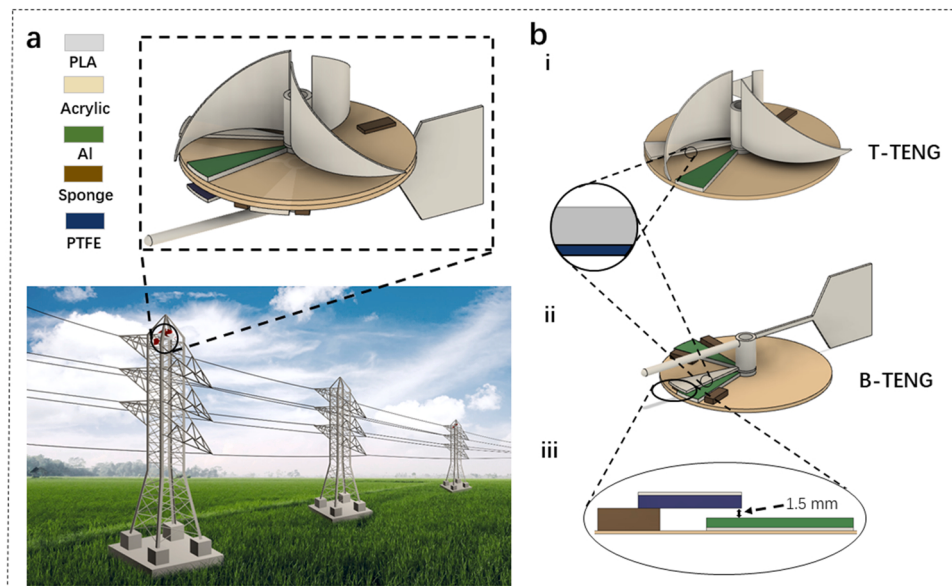
### 2.3. Signal processing and system implementation

The signal acquisition, timing synchronization and graphical user interface are implemented using NI DAQ-mx, LabVIEW Runtime engine and C# programming language.

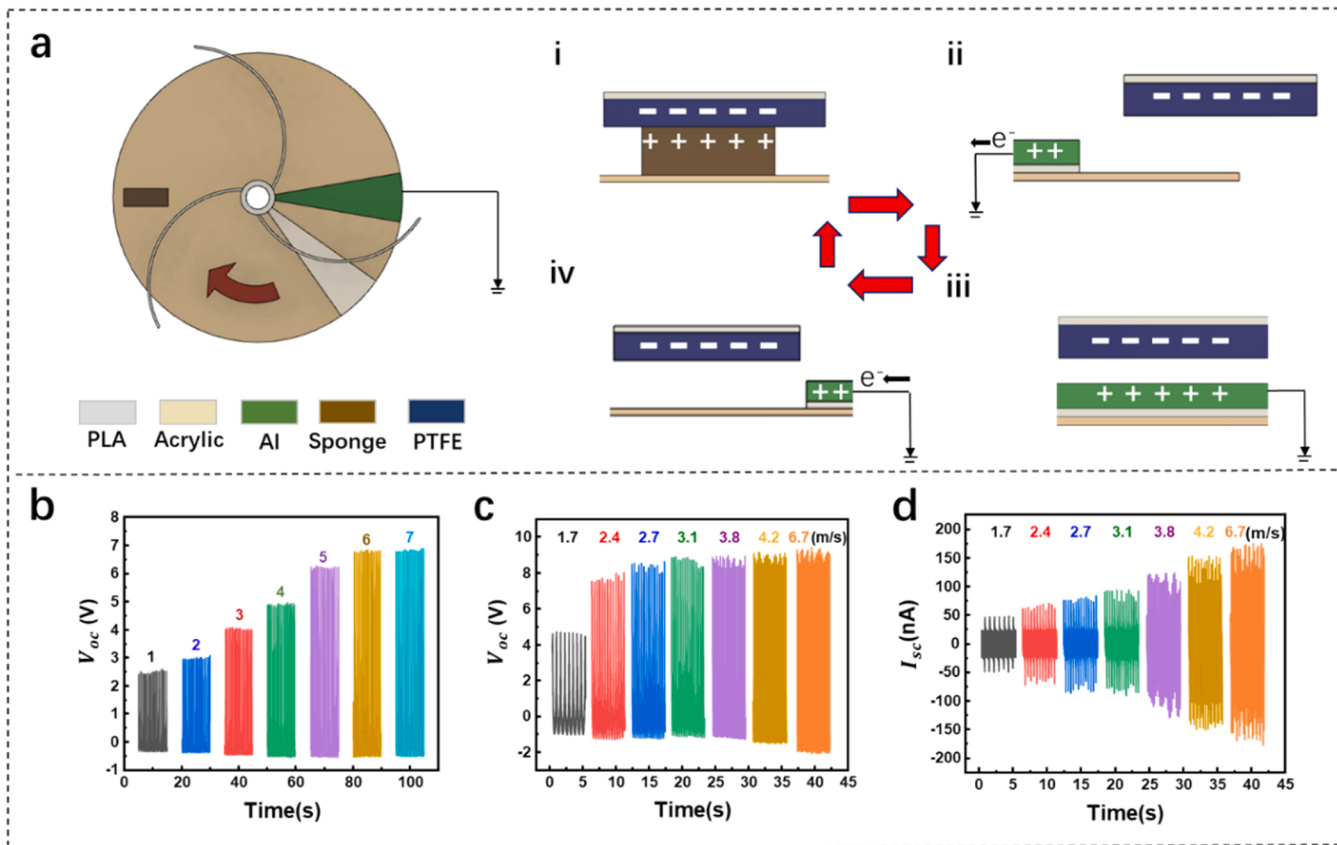
## 3. Results and discussions

Fig. 1 shows the design of WM-TENG, which consists of a top TENG (T-TENG) for measuring wind speed and a bottom TENG (B-TENG) for monitoring wind direction. As shown in Fig. 1a, the WM-TENG can be deployed on a transmission tower. The two parts of WM-TENG, T-TENG and B-TENG both contain a moving part and a fixed part, as represented in Fig. 1b. T-TENG's turbine blades can collect wind energy to drive its moving part to rotate. The Al electrode is fixed on acrylic substrate, and the sponge (8 mm × 20 mm) is pasted in the opposite position. Through the optimized design of turbine blades and sleeve, T-TENG has a minimum start-up wind speed of 1.7 m/s. The wind vane of B-TENG can drive its moving part to do circular movement or swing near the electrode to reflect the wind direction under various scenarios, as shown in Fig. 1b (ii). Two connected Al electrodes are used to determine the range of the wind direction to be monitored, and each electrode has sponges attached to its both sides. During the movement, there is always a distance of 1.5 mm in vertical direction between PTFE and Al electrodes both in T-TENG and B-TENG, as illustrated in Fig. 1b(iii) and Fig. S3. Due to the charge dissipation caused by non-contact, sponges are used to replenish the additional charges. With this design, material abrasions can be reduced and the lifetime of WM-TENG is extended.

Fig. 2a shows the working mechanism of T-TENG as it rotates along its shaft, which consists of two main processes, the triboelectric charging between PTFE and sponge and the electrostatic induction between PTFE and Al electrodes, respectively. Initially, the surface of PTFE is not charged. When the surface of PTFE is in contact with sponge, due to their different electrical polarities and triboelectric charging effect, PTFE attracts electrons from sponge, resulting negatively charged PTFE surface and positively charged sponge surface with equal amount of charges, as illustrated in (i). Because of the inherent electret properties of PTFE, the triboelectric charges on its surface can persist for a long time to enable electrostatic induction [42,43]. In (ii), as the negatively charged PTFE leaves sponge and approaches the Al electrode, since the electrode is connected to the earth, electrons flow from Al electrode to the ground in order to maintain charge equilibrium, resulting in a positive current. As the moving part of T-TENG continues to rotate, it reaches state (iii) when PTFE and Al electrode are completely overlapped. At this moment, the induced electric potential reaches its maximum value. Subsequently, the PTFE starts to move away from Al electrode and electrons flow back



**Fig. 1.** Structural design and application scenarios of WM-TENG. (a) Schematic diagram of the integrated wind sensor system and its application scenarios. (b) Wind sensor consisting of (i) T-TENG for wind speed measuring and (ii) B-TENG for wind direction monitor. (iii) Side view illustrating the induction distance between PTFE and Al.



**Fig. 2.** Working mechanism and output characteristics of T-TENG for measuring wind speed. (a) Structure and working mechanism of T-TENG for power generation. (b) Output voltage versus rotating period at wind speed of 2 m/s. The seven measured periods with each period of 10 s start from timing points of 10 s, 110 s, 210 s, 310 s, 9 min, 12 min and 15 min, respectively. (c) The open-circuit voltage and (d) short-circuit current of the non-contact T-TENG.

from the ground, generating a negative current, as shown in state (iv). In this cycle, the PTFE on the moving part is not in contact with Al electrodes, and the current generation process relies entirely on the mutual induction between PTFE and Al electrodes.

The output performance of T-TENG is shown in Fig. 2b-d and the data collection platform used in this work is shown in Fig. S4a. Under the condition that the wind speed is fixed at 2 m/s, the open-circuit voltage  $V_{oc}$  of T-TENG during long-term rotation process is investigated. The initial  $V_{oc}$  measuring points starts from 10 s, 110 s, 210 s, 310 s, 9 min, 12 min and 15 min, and for each measurement, it takes 10 s. These results in Fig. 2b demonstrate that the  $V_{oc}$  of T-TENG gradually increases with rotation time and stabilizes at 6.8 V after T-TENG rotates for 12 min. This is due to the fact that the surface charge density  $\rho_{sc}$  of PTFE changes from low to high and finally reaches its saturated value after multiple contact electrification with sponge, while the amount of induced charges on Al electrode is always positively correlated with  $\rho_{sc}$ . To further accurately analyze the relationship between the output signal and wind speed, the steady-state outputs of T-TENG rotating at different wind speeds are investigated. Fig. 2c-d indicate the dependance of  $V_{oc}$  and short-circuit current  $I_{sc}$  of T-TENG with wind speed ranging from 1.7 m/s to 6.7 m/s. As shown in Fig. 2c,  $V_{oc}$  increases rapidly at first, and then tends to be stable after the wind speed reaches 2.7 m/s. This observation indicates that when T-TENG is driven by high wind speed, the  $\rho_{sc}$  of PTFE can be easily maximized due to the more frequent occurrences of triboelectric effect. According to the theory of TENG, it can be considered as a constant capacitor that performs periodic charging and discharging. The more frequent process for triboelectric and electrostatic induction, the less time to transfer equal charges, resulting in a higher current. That is, as shown in Fig. 2d, the  $I_{sc}$  of T-TENG increases with wind speed and reaches an output of 168 nA at wind speed of

6.7 m/s. In addition, a programmable software is designed and implemented to measure the current wind speed by analyzing voltage signal frequency of T-TENG in real time. Fig. S4b is a software screenshot of the T-TENG output operating at wind speed of 2.6 m/s.

To continuously monitor wind blowing directions which could cause weak wind vibrations on electric transmission lines, two fixed electrodes are connected and placed symmetrically on B-TENG. When wind blow on the moving part, the PTFE film contacts with Al electrode, generating electrical signals. These different signals correspond to the movement trajectory of the moving parts of B-TENG, further reflecting the change of wind directions. First, the compensation effect of the sponges on triboelectric charge is studied. Fig. S5 shows the  $V_{oc}$  output of B-TENG when the number of the sponges N is 0, 2, and 4, respectively. When N is 0,  $V_{oc}$  is almost zero. This is because PTFE does not contact with the sponge, resulting in a weak or even undetectable electrostatic induction effect between PTFE and Al. Increasing N from 0 to 2 and 4 helps generate more charges on the PTFE surfaces because of more contact electrification between the sponge and PTFE. To simplify the structure and ensure sufficient charge distribution on PTFE at the same time, the experiments are performed using B-TENG with 2 or 4 sponges. Fig. 3a shows the experiment setup of the back-and-forth movement of PTFE from the outside to the area between the two Al electrodes. As can be seen from Fig. 3b, during the process of PTFE approaching the Al electrodes from the outside (i) to fully overlap with one electrode (ii),  $V_{oc}$  gradually increases and reaches its maximum value. When PTFE moves away from the overlapped Al electrode, the changing trend of  $V_{oc}$  is different between two moving directions, i.e., when it goes towards the area between the two electrodes (ii-iii) and when it moves towards to the outside (ii-i). When PTFE is between the two electrodes (iii),  $V_{oc}$  does not drop to 0 V but stabilizes around a middle value of 4 V. At this time, the

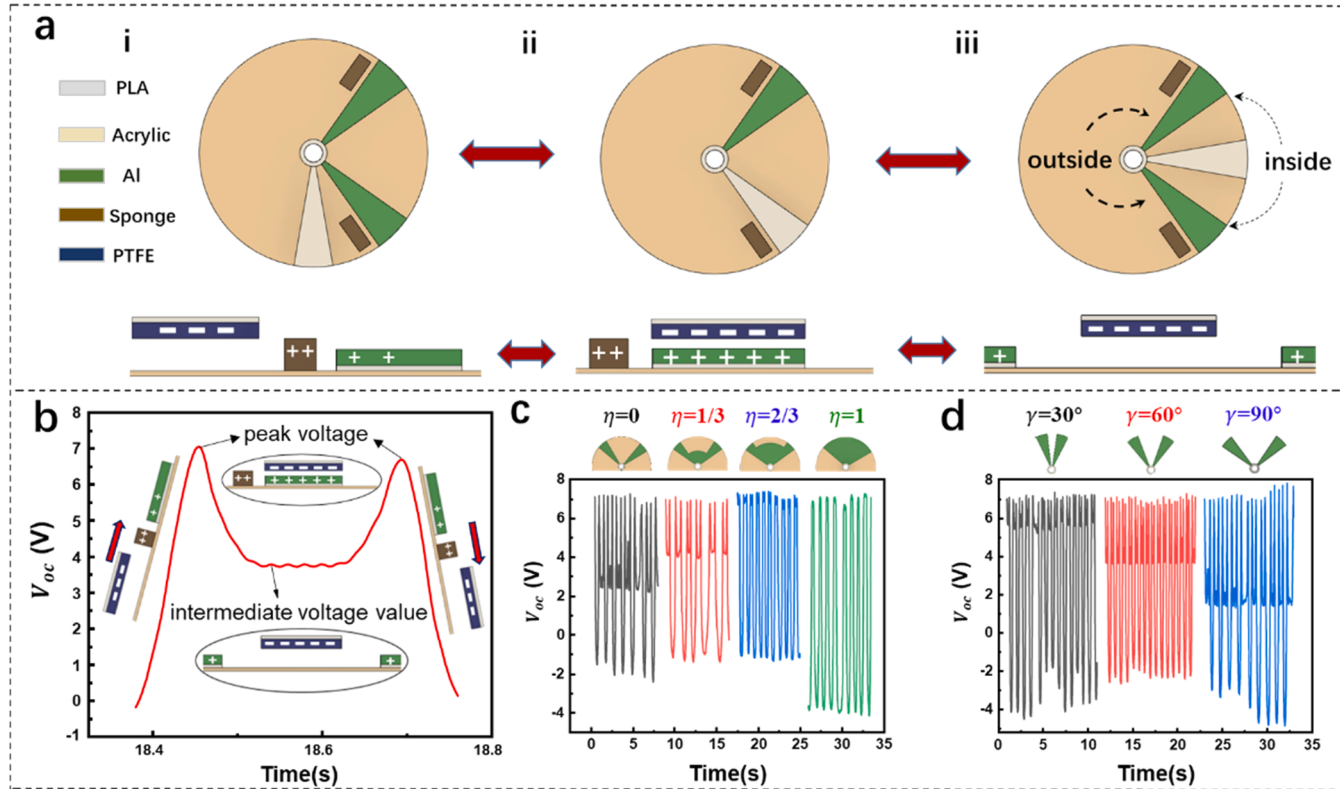


**Fig. 3.** Mechanism of B-TENG for wind direction detection. (a) Movement diagram of the moving part of B-TENG. (b) The  $V_{oc}$  output of B-TENG ( $N = 2$ ,  $\eta=0$  and angle  $\gamma=60^\circ$ ). (c)  $V_{oc}$  output signal with different connection area  $\eta$  and (d) angle  $\gamma$  between two electrodes.

representative wind direction is within the monitoring range, and the electrical signal can be extracted for time-scale analysis. This voltage is called "intermediate voltage value  $V_{IM}$ ".

The effect of two geometric parameters on  $V_{IM}$  is investigated: the connection area ratio  $\eta$  and the angle  $\gamma$  between two Al electrodes. Fig. 3c shows  $V_{oc}$  of B-TENG when the parameter  $\eta$  is 0, 1/3, 2/3 and 1, respectively. The positive peaks of  $V_{oc}$  are almost the same for all different  $\eta$ . The value of  $V_{IM}$  increases with the increase of  $\eta$ . When  $\eta$  is equal to 1,  $V_{IM}$  approaches the positive peaks of  $V_{oc}$  as the Al electrode becomes a complete sector and the overlapping area of PTFE and Al does not change until PTFE further rotates into the outside area. Therefore, to analyze  $V_{IM}$  clearly from  $V_{oc}$ ,  $\eta$  should converge to 0. Next, when the parameter  $\gamma$  is set to  $30^\circ$ ,  $60^\circ$  and  $90^\circ$ , respectively, the peak values of  $V_{oc}$  are always around 7 V, as illustrated in Fig. 3d. However,  $V_{IM}$  significantly decreases with increasing  $\gamma$ . This is because when the PTFE is located in the middle of the two electrodes, the increased  $\gamma$  makes the distance of charge induction increase, resulting in a decrease in the induced charges and leading to a decrease in  $V_{IM}$ . It can be inferred that the appearance of intermediate voltage is due to the fact that when PTFE is between the two connected Al electrodes, the contact area between the PTFE and Al electrode is relatively unchanged, and the induced charges on the Al electrode does not change too much with the wiggling of PTFE between the two Al electrodes. Thus the  $V_{IM}$  keeps relatively stable.

To analyze the influence of different rotation speed on  $V_{IM}$ , we measured  $V_{oc}$  output signals under slow and fast rotation speed, respectively, as shown in Fig. 4a. When B-TENG rotates slowly, the  $t_1$  represents the process of the moving parts rotating from the outside to the inside. When the moving part overlaps with the first aluminum electrode, it stays for 6 s. Then it continues to rotate and stays in the middle position of the two electrodes for  $t_2$  of 6 s. During  $t_3$ , the PTFE slips out slowly without staying in the middle of the two electrodes. When B-TENG rotates rapidly, the time  $t_4$  and  $t_6$  for PTFE to sweep

across the Al electrode is only 0.2 s. The  $V_{IM}$  duration  $t_5$  is only 0.7 s. Comparing the two processes at different speeds, the peak value of  $V_{oc}$  and  $V_{IM}$  are the same and neither is affected by the speed of the rotation. The frequency and value of  $I_{sc}$  increase with the increase of rotational speed (Fig. 4b). After the geometric parameters of the B-TENG are determined, the  $V_{IM}$  can avoid the influence of the rotational speed, indicating that the wind direction is within the monitoring range. The time span of  $V_{IM}$  can be used to record information of breeze vibration on transmission lines. The monitoring program used to visualize the results and real-time signal is shown in Fig. S6.

Due to the instability and uncertainty of environmental wind, the actual operation of B-TENG in reality is much more complicated. We here simulate five operational situations that could occur in natural environment to study the practicability and accuracy of this sensor device, as shown in Fig. 4c. Case 1 shows that the PTFE rotates from the outside to the middle of the two electrodes, and then moves back and forth. The speed is constantly increasing. It can be clearly observed that the frequency of the electrical signal becomes faster and the time period of the intermediate voltage value decreases. It is shown that there is no effect on the peak and intermediate voltage of the output signal even in the case of variable rotating speed. Case 2 reflects the PTFE oscillating between the two Al electrodes and compares the change of wind direction within the monitored range and near the boundary. Every time  $V_{IM}$  has obvious fluctuations, indicating that the PTFE and Al electrode overlap. Case 3 shows that the peak value increases with the increase of overlapping area between the PTFE and Al electrodes. Case 4 illustrates different signal outputs of PTFE rotating from the inside of the Al electrode to hovering just above the Al electrode. Their values are all greater than the peak values in Case 3. The length of the duration of the wind direction at the boundary can be calculated from the corresponding signal. Case 5 represents PTFE returning from the above electrode to the outside and oscillating around the outside and the boundary, and in this case, although the peak voltage is similar, there is no intermediate

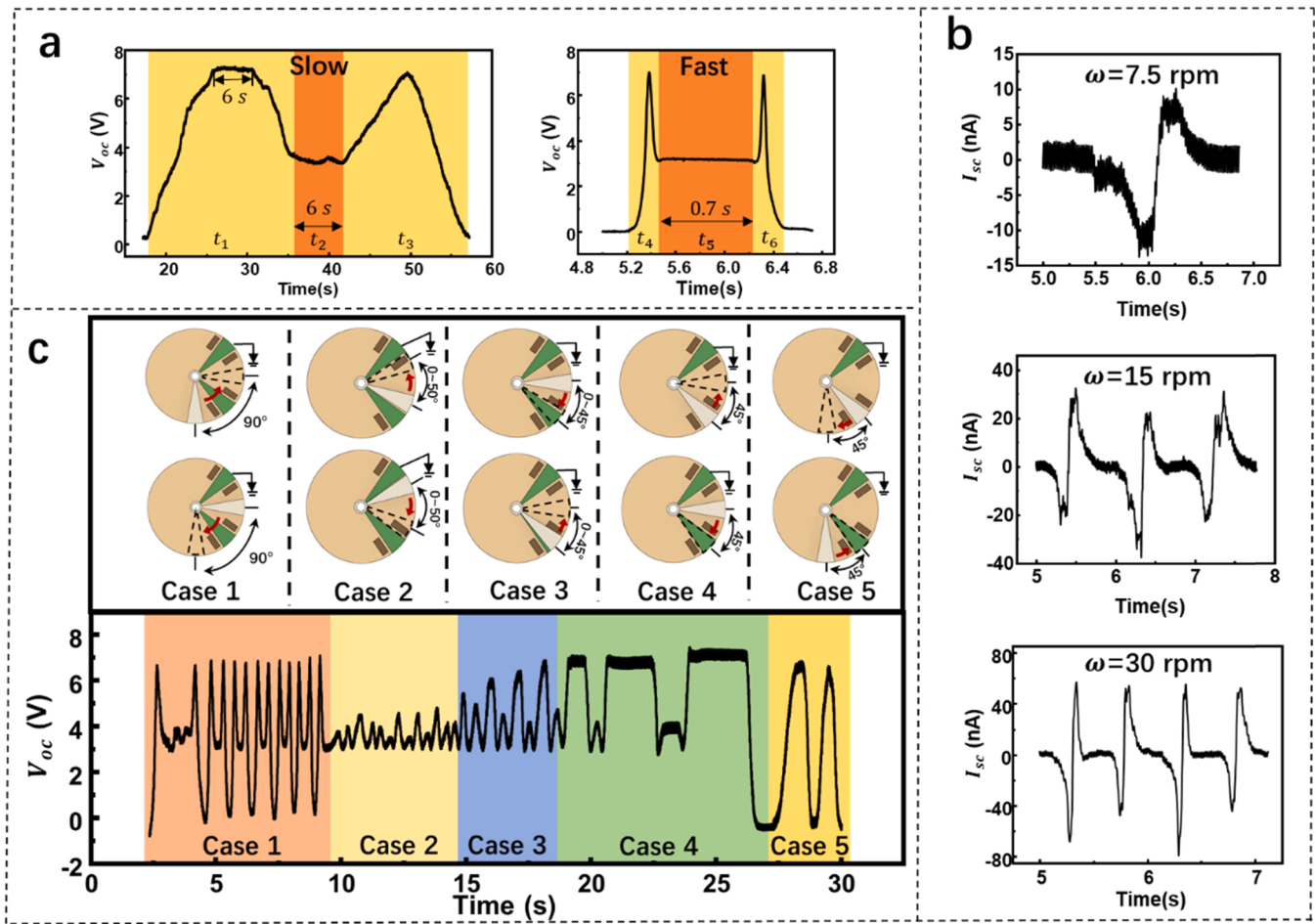


**Fig. 4.** (a) The  $V_{oc}$  output of B-TENG under fast and slow rotation speeds. (b) The relationship of  $I_{sc}$  output of B-TENG with different rotation speeds. (c) The motion of moving part and the recorded  $V_{oc}$  output of B-TENG in five cases of wind direction.

voltage value. It shows that the intermediate voltage can clearly distinguish whether the wind direction is within the monitored range. In the four boundary-related situations simulated by Case 2, 3, 4, and 5, B-TENG can identify different output signals, and can even deduce the change of wind direction through the analysis of obtained output signals.

To demonstrate the feasibility of WM-TENG, a wind monitoring

system for electric transmission lines is designed and demonstrated. The electrode part is encapsulated with a fabricated shielding case, as shown in Fig. S7, which can greatly reduce the interference of the surrounding electric and magnetic field [44]. The breeze vibration on transmission lines can be induced only when wind speed and direction meet the natural conditions mentioned above at the same time. Therefore, the two parts need to cooperate with each other to complete wind

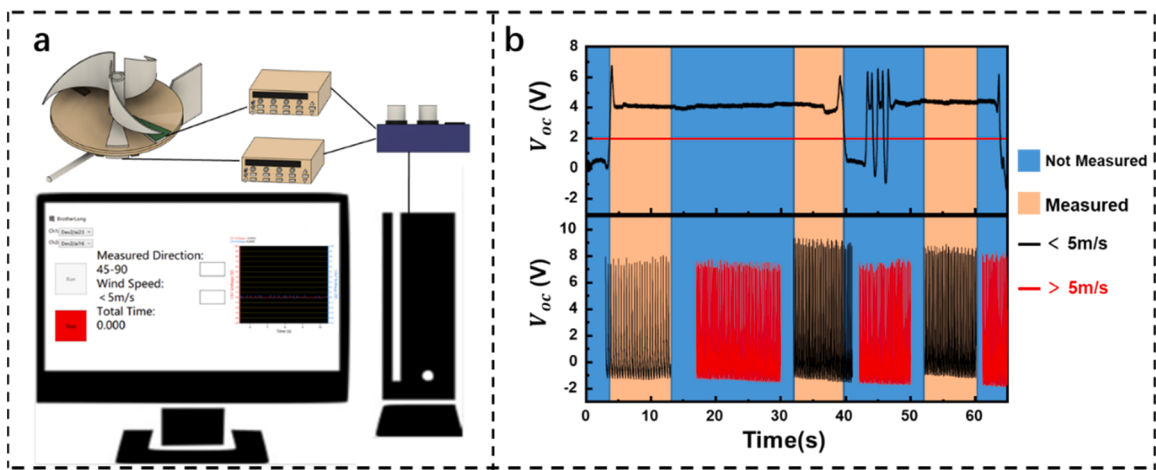


**Fig. 5.** (a) The visualization of data measuring and process for wind detection. (b) Schematic diagram of output analysis when wind direction (top) and wind speed (bottom) are monitored together.

monitoring. Fig. 5a is the test platform of the monitoring system in the experiment. The top and bottom section in Fig. 5b show the corresponding signals of wind direction and wind speed, respectively. In the bottom section, the red line represents the output signal generated by wind speed greater than 5 m/s, and the black one corresponds to the wind speed of 1.7–5 m/s. The measured timespan only starts when two conditions are both satisfied, for example, the orange background indicates the timespan satisfying the recording requirements, while the blue one does not. This design can only monitor the wind direction from one side. Due to the electrostatic induction between PTFE and Al electrodes, if a pair of symmetrical fixed electrode is deployed on the other side to monitor the wind direction on both sides, as shown in Fig. S8, no matter where the PTFE is located, the charges will be induced on both sides of electrodes. Therefore, in actual use, another symmetrical device is required to complete the wind direction monitoring on both sides.

#### 4. Conclusions

In conclusion, a self-powered wind sensor based on WM-TENG is designed for monitoring wind speed and wind direction that cause breeze vibration on overhead transmission lines. A non-contact design with sponges is used to reduce the abrasion existed in traditional TENG and provide polarized charges. The results show that the T-TENG can measure wind speed ranging from 1.7 m/s to 6.7 m/s, and the appearance of the intermediate voltage can assist the B-TENG to distinguish the wind direction. Finally, the breeze vibration time on transmission lines is recorded and analyzed by the statistical  $V_{oc}$  results combined with a home designed software. The proposed WM-TENG has the ability to monitor wind information without external power source, and more importantly, provides a new strategy for breeze vibration monitoring on transmission lines to solve the power supply challenges of grid sensors.

#### CRediT authorship contribution statement

**Xiaolong Tang:** Conceptualization, Methodology, Visualization, Data curation, Writing – original draft. **Wenchi Hou:** Methodology, Visualization, Validation. **Qiwei Zheng:** Methodology, Validation. **Lin Fang:** Methodology, Data curation. **Rui Zhu:** Resources, Conceptualization. **Li Zheng:** Resources, Conceptualization, Methodology, Supervision, Writing – review & editing.

#### Declaration of Competing Interest

The authors declare that they have no known competing financial interests or personal relationships that could have appeared to influence the work reported in this paper.

#### Acknowledgements

The work was supported by National Natural Science Foundation of China (Grant No. 12172210), the Program for Professor of Special Appointment (Eastern Scholar) (TP2017076) at Shanghai Institutions of Higher Learning, Science and Technology Commission of Shanghai Municipality (19DZ2271100).

#### Appendix A. Supporting information

Supplementary data associated with this article can be found in the online version at [doi:10.1016/j.nanoen.2022.107412](https://doi.org/10.1016/j.nanoen.2022.107412).

#### References

- [1] A.J. Lamadrid, S. Maneevitijit, T.D. Mount, The economic value of transmission lines and the implications for planning models, *Energy Econ.* 57 (2016) 1–15, <https://doi.org/10.1016/j.eneco.2016.03.015>.
- [2] Þ. Stefánsson, A.D. Sæþórssdóttir, C.M. Hall, When tourists meet transmission lines: the effects of electric transmission lines on tourism in Iceland, *Energy Res. Soc. Sci.* 34 (2017) 82–92, <https://doi.org/10.1016/j.erss.2017.06.032>.
- [3] T. Magier, M. Tenzer, H. Koch, Direct current gas-insulated transmission lines, *IEEE Trans. Power Deliv.* 33 (2018) 440–446, <https://doi.org/10.1109/TPWRD.2017.2716182>.
- [4] Y.D. Kubelwa, A.G. Swanson, K.O. Papailiou, D.G. Dorrell, On the Euler-lagrange formalism to compute power line bundle conductors subject to aeolian vibrations, *Mech. Syst. Signal Process.* 163 (2022), 108099, <https://doi.org/10.1016/j.ymssp.2021.108099>.
- [5] H. Wu, J. Wang, Z. Wu, S. Kang, X. Wei, H. Wang, H. Luo, L. Yang, R. Liao, Z. L. Wang, Multi-parameter optimized triboelectric nanogenerator based self-powered sensor network for broadband aeolian vibration online-monitoring of transmission lines, *Adv. Energy Mater.* 12 (2022), 2103654, <https://doi.org/10.1002/aenm.202103654>.
- [6] J. Liu, B. Yan, Z. Mou, Y. Gao, G. Niu, X. Li, Numerical study of aeolian vibration characteristics and fatigue life estimation of transmission conductors, *PLOS ONE* 17 (2022), e0263163, <https://doi.org/10.1371/journal.pone.0263163>.
- [7] L. Zhao, X. Huang, Y. Zhao, W. Si, Design of a wireless vibration metre for conductor vibration monitoring, *Struct. Control Health Monit.* 25 (2018), e2143, <https://doi.org/10.1002/stc.2143>.
- [8] F. Foti, L. Martinelli, A unified analytical model for the self-damping of stranded cables under aeolian vibrations, *J. Wind Eng. Ind. Aerodyn.* 176 (2018) 225–238, <https://doi.org/10.1016/j.jweia.2018.03.028>.
- [9] L. Zhao, X. Huang, Y. Zhang, Y. Zhu, J. Jia, C. Zhu, Aeolian vibration-based structural health monitoring system for transmission line conductors, *Struct. Control Health Monit.* 27 (2020), <https://doi.org/10.1002/stc.2538>.
- [10] M.H. Cho, J. Trottier, C. Gagnon, P. Hovington, D. Clément, A. Vijh, C.-S. Kim, A. Guerfi, R. Black, L. Nazar, K. Zaghib, The effects of moisture contamination in the Li-O<sub>2</sub> battery, *J. Power Sources* 268 (2014) 565–574, <https://doi.org/10.1016/j.jpowsour.2014.05.148>.
- [11] Y. Chen, Z. Gao, F. Zhang, Z. Wen, X. Sun, Recent progress in self-powered multifunctional e-skin for advanced applications, *Exploration* 2 (2022), 20210112, <https://doi.org/10.1002/EXP.20210112>.
- [12] Q. Zheng, L. Fang, X. Tang, L. Zheng, H. Li, Indoor air dust removal system based on high-voltage direct current triboelectric nanogenerator, *Nano Energy* 97 (2022), 107183, <https://doi.org/10.1016/j.nanoen.2022.107183>.
- [13] X. Zhong, Y. Yang, X. Wang, Z.L. Wang, Rotating-disk-based hybridized electromagnetic-triboelectric nanogenerator for scavenging biomechanical energy as a mobile power source, *Nano Energy* 13 (2015) 771–780, <https://doi.org/10.1016/j.nanoen.2015.03.012>.
- [14] Z.L. Wang, Catch wave power in floating nets, *Nature* 542 (2017) 159–160, <https://doi.org/10.1038/542159a>.
- [15] Y. Wang, X. Yu, M. Yin, J. Wang, Q. Gao, Y. Yu, T. Cheng, Z.L. Wang, Gravity triboelectric nanogenerator for the steady harvesting of natural wind energy, *Nano Energy* 82 (2021), 105740, <https://doi.org/10.1016/j.nanoen.2020.105740>.
- [16] X. Lu, H. Zhang, X. Zhao, H. Yang, L. Zheng, W. Wang, C. Sun, Triboelectric nanogenerator based self-powered sensor with a turnable sector structure for monitoring driving behavior, *Nano Energy* 89 (2021), 106352, <https://doi.org/10.1016/j.nanoen.2021.106352>.
- [17] L. Fang, Q. Zheng, W. Hou, L. Zheng, H. Li, A self-powered vibration sensor based on the coupling of triboelectric nanogenerator and electromagnetic generator, *Nano Energy* 97 (2022), 107164.
- [18] H. Lei, K. Cao, Y. Chen, Z. Liang, Z. Wen, L. Jiang, X. Sun, 3D-printed endoplasmic reticulum rGO microstructure based self-powered triboelectric pressure sensor, *Chem. Eng. J.* 445 (2022), 136821, <https://doi.org/10.1016/j.cej.2022.136821>.
- [19] Z. Yan, L. Wang, Y. Xia, R. Qiu, W. Liu, M. Wu, Y. Zhu, S. Zhu, C. Jia, M. Zhu, R. Cao, Z. Li, X. Wang, Flexible high-resolution triboelectric sensor array based on patterned laser-induced graphene for self-powered real-time tactile sensing, *Adv. Funct. Mater.* 31 (2021), 2100709, <https://doi.org/10.1002/adfm.202100709>.
- [20] H. Zhang, Y. Yang, T.-C. Hou, Y. Su, C. Hu, Z.L. Wang, Triboelectric nanogenerator built inside clothes for self-powered glucose biosensors, *Nano Energy* 2 (2013) 1019–1024, <https://doi.org/10.1016/j.nanoen.2013.03.024>.
- [21] S. Li, D. Liu, Z. Zhao, L. Zhou, X. Yin, X. Li, Y. Gao, C. Zhang, Q. Zhang, J. Wang, Z. L. Wang, A fully self-powered vibration monitoring system driven by dual-mode triboelectric nanogenerators, *ACS Nano* 14 (2020) 2475–2482, <https://doi.org/10.1021/acsnano.9b10142>.
- [22] C. Li, Y. Yin, B. Wang, T. Zhou, J. Wang, J. Luo, W. Tang, R. Cao, Z. Yuan, N. Li, X. Du, C. Wang, S. Zhao, Y. Liu, Z.L. Wang, Self-powered electrospinning system driven by a triboelectric nanogenerator, *ACS Nano* 11 (2017) 10439–10445, <https://doi.org/10.1021/acsnano.7b05626>.
- [23] C. Chen, Z. Wen, J. Shi, X. Jian, P. Li, J.T.W. Yeow, X. Sun, Micro triboelectric ultrasonic device for acoustic energy transfer and signal communication, *Nat. Commun.* 11 (2020) 4143, <https://doi.org/10.1038/s41467-020-17842-w>.
- [24] M. Wu, X. Wang, Y. Xia, Y. Zhu, S. Zhu, C. Jia, W. Guo, Q. Li, Z. Yan, Stretchable freezing-tolerant triboelectric nanogenerator and strain sensor based on transparent, long-term stable, and highly conductive gelatin-based organohydrogel, *Nano Energy* 95 (2022), 106967, <https://doi.org/10.1016/j.nanoen.2022.106967>.
- [25] Y. Zhu, Y. Xia, M. Wu, W. Guo, C. Jia, X. Wang, Wearable, freezing-tolerant, and self-powered electroluminescence system for long-term cold-resistant displays, *Nano Energy* 98 (2022), 107309.
- [26] L. Wang, W. Liu, Z. Yan, F. Wang, X. Wang, Stretchable and shape-adaptable triboelectric nanogenerator based on biocompatible liquid electrolyte for biomechanical energy harvesting and wearable human-machine interaction, *Adv. Funct. Mater.* 31 (2021), 2007221, <https://doi.org/10.1002/adfm.202007221>.

- [27] X. Fu, S. Xu, Y. Gao, X. Zhang, G. Liu, H. Zhou, Y. Lv, C. Zhang, Z.L. Wang, Breeze-wind-energy-powered autonomous wireless anemometer based on rolling contact-electrification, *ACS Energy Lett.* 6 (2021) 2343–2350, <https://doi.org/10.1021/acsenergylett.1c00704>.
- [28] X. Li, Y. Cao, X. Yu, Y. Xu, Y. Yang, S. Liu, T. Cheng, Z.L. Wang, Breeze-driven triboelectric nanogenerator for wind energy harvesting and application in smart agriculture, *Appl. Energy* 306 (2022), 117977, <https://doi.org/10.1016/j.apenergy.2021.117977>.
- [29] H.-X. Zou, L.-C. Zhao, Q. Wang, Q.-H. Gao, G. Yan, K.-X. Wei, W.-M. Zhang, A self-regulation strategy for triboelectric nanogenerator and self-powered wind-speed sensor, *Nano Energy* 95 (2022), 106990, <https://doi.org/10.1016/j.nanoen.2022.106990>.
- [30] Y. Yang, G. Zhu, H. Zhang, J. Chen, X. Zhong, Z.-H. Lin, Y. Su, P. Bai, X. Wen, Z. L. Wang, Triboelectric nanogenerator for harvesting wind energy and as self-powered wind vector sensor system, *ACS Nano* 7 (2013) 9461–9468, <https://doi.org/10.1021/nn4043157>.
- [31] M. Xu, Y.-C. Wang, S.L. Zhang, W. Ding, J. Cheng, X. He, P. Zhang, Z. Wang, X. Pan, Z.L. Wang, An aeroelastic flutter based triboelectric nanogenerator as a self-powered active wind speed sensor in harsh environment, *Extrem. Mech. Lett.* 15 (2017) 122–129, <https://doi.org/10.1016/j.eml.2017.07.005>.
- [32] X. Li, Y. Li, M. Zhang, Z. Yang, K. Wang, C. Huang, Carbon nano thorn arrays based water/cold resisted nanogenerator for wind energy harvesting and speed sensing, *Nano Energy* 90 (2021), 106571, <https://doi.org/10.1016/j.nanoen.2021.106571>.
- [33] Q. Han, Z. Ding, W. Sun, X. Xu, F. Chu, Hybrid triboelectric-electromagnetic generator for self-powered wind speed and direction detection, *Sustain. Energy Technol. Assess.* 39 (2020), 100717, <https://doi.org/10.1016/j.seta.2020.100717>.
- [34] J. Wang, W. Ding, L. Pan, C. Wu, H. Yu, L. Yang, R. Liao, Z.L. Wang, Self-powered wind sensor system for detecting wind speed and direction based on a triboelectric nanogenerator, *ACS Nano* 12 (2018) 3954–3963, <https://doi.org/10.1021/acsnano.8b01532>.
- [35] Y. Wang, E. Yang, T. Chen, J. Wang, Z. Hu, J. Mi, X. Pan, M. Xu, A novel humidity resisting and wind direction adapting flag-type triboelectric nanogenerator for wind energy harvesting and speed sensing, *Nano Energy* 78 (2020), 105279, <https://doi.org/10.1016/j.nanoen.2020.105279>.
- [36] Z. Zhao, B. Wei, Y. Wang, X. Huang, B. Li, F. Lin, L. Ma, Q. Zhang, Y. Zou, F. Yang, H. Pang, J. Xu, X. Pan, An array of flag-type triboelectric nanogenerators for harvesting wind energy, *Nanomaterials* 12 (2022) 721, <https://doi.org/10.3390/nano12040721>.
- [37] T. Zhao, S. Cao, S. Yang, R. Guo, S. Sang, H. Zhang, A self-powered counter/timer based on a clock pointer-like frequency-tunable triboelectric nanogenerator for wind speed detecting, *Nano Energy* 65 (2019), 104025, <https://doi.org/10.1016/j.nanoen.2019.104025>.
- [38] J. Liu, Z. Wen, H. Lei, Z. Gao, X. Sun, A liquid-solid interface-based triboelectric tactile sensor with ultrahigh sensitivity of  $21.48 \text{ kPa}^{-1}$ , *Nano-Micro Lett.* 14 (2022) 88.
- [39] S. Li, S. Wang, Y. Zi, Z. Wen, L. Lin, G. Zhang, Z.L. Wang, Largely improving the robustness and lifetime of triboelectric nanogenerators through automatic transition between contact and noncontact working states, *ACS Nano* 9 (2015) 7479–7487, <https://doi.org/10.1021/acsnano.5b02575>.
- [40] S. Wang, Y. Xie, S. Niu, L. Lin, Z.L. Wang, Freestanding triboelectric-layer-based nanogenerators for harvesting energy from a moving object or human motion in contact and non-contact modes, *Adv. Mater.* 26 (2014) 2818–2824, <https://doi.org/10.1002/adma.201305303>.
- [41] X. Kong, Y. Liu, Y. Liu, Y. Zheng, D. Wang, B. Wang, C. Xu, D. Wang, New coating TENG with antiwear and healing functions for energy harvesting, *ACS Appl. Mater. Interfaces* 12 (2020) 9387–9394, <https://doi.org/10.1021/acsami.9b22649>.
- [42] J. Chen, Z.L. Wang, Reviving vibration energy harvesting and self-powered sensing by a triboelectric nanogenerator, *Joule* 1 (2017) 480–521, <https://doi.org/10.1016/j.joule.2017.09.004>.
- [43] H. Guo, X. Pu, J. Chen, Y. Meng, M.-H. Yeh, G. Liu, Q. Tang, B. Chen, D. Liu, S. Qi, C. Wu, C. Hu, J. Wang, Z.L. Wang, A highly sensitive, self-powered triboelectric auditory sensor for social robotics and hearing aids, *Sci. Robot.* 3 (2018) eaat2516, <https://doi.org/10.1126/scirobotics.aat2516>.
- [44] X. Zhao, X. Lu, Q. Zheng, L. Fang, L. Zheng, X. Chen, Z.L. Wang, Studying of contact electrification and electron transfer at liquid-liquid interface, *Nano Energy* 87 (2021), 106191, <https://doi.org/10.1016/j.nanoen.2021.106191>.